Monte Carlo simulation of monolayer graphene at nonzero temperature

Wesley Armour,[1,2] Simon Hands,[3] and Costas Strouthos[4]

[1]*Diamond Light Source, Harwell Campus, Didcot, Oxfordshire OX11 0DE, United Kingdom*

[2]*Institute for the Future of Computing, Oxford Martin School, Oxford e-Research Centre, 7 Keble Road, Oxford OX1 3QG, United Kingdom*

[3]*Department of Physics, College of Science, Swansea University, Singleton Park, Swansea SA2 8PP, United Kingdom*

[4]*Computation-based Science and Technology Research Center, The Cyprus Institute, 1645 Nicosia, Cyprus*

(Received 13 May 2011; published 8 August 2011)

We present results from lattice simulations of a monolayer graphene model at nonzero temperature. At low temperatures for sufficiently strong coupling the model develops an excitonic condensate of particle-hole pairs corresponding to an insulating phase. The Berezinskii-Kosterlitz-Thouless phase transition temperature is associated with the value of the coupling where the critical exponent δ governing the response of the order parameter at criticality to an external source has a value close to 15. The critical coupling on a lattice with temporal extent $N_t = 32$ [$T = 1/(N_t a_t)$ where a_t is the temporal lattice spacing] and spatial extent $N_s = 64$ is very close to infinite coupling. The value of the transition temperature normalized with the zero-temperature fermion mass gap Δ_0 is given by $\frac{T_{\mathrm{BKT}}}{\Delta_0} = 0.055(2)$. This value provides an upper bound on the transition temperature, because simulations closer to the continuum limit where the full U(4) symmetry is restored may result in an even lower value. In addition, we measured the helicity modulus Υ and the fermion thermal mass $\Delta_T(T)$, the latter providing evidence for a pseudogap phase with $\Delta_T > 0$ extending to arbitrarily high T. Analysis of the dispersion relation suggests that the Fermi velocity is not sensitive to thermal effects.

DOI: 10.1103/PhysRevB.84.075123 PACS number(s): 11.10.Kk, 11.15.Ha, 71.10.Fd, 73.63.Bd

I. INTRODUCTION

The impact of electron-electron interactions on the physics of graphene is an important focus of current study (for recent reviews, see Ref. 1). There are simple arguments as to why an "independent quasiparticle" picture may not be adequate for certain properties. First, since the carrier density of states vanishes in undoped graphene (the zero-energy condition is only satisfied at two isolated "Dirac points" in the first Brillouin zone), the effects of screening are much less in graphene than in a conventional conductor, the main contribution coming from electron-hole pairs which increase the effective dielectric constant of the medium in a fashion entirely analogous to vacuum polarization in QED. This means that the interaction between charged carriers remains Coulombic, that is, long-ranged $\propto r^{-1}$. Second, the relative importance of quantum corrections, parametrized by the fine structure constant α, is much greater than in conventional QED, because $\alpha_{\mathrm{eff}} = \frac{e^2}{4\pi\varepsilon\hbar v_F}$, where $v_F \approx \frac{c}{300}$ is the Fermi velocity and ε the dielectric permittivity of the underlying substrate: Hence, $\alpha_{\mathrm{eff}} = \alpha\frac{c}{v_F} \sim O(1)$, and its value depends on the substrate, taking a maximum value 2.16 for suspended graphene.

These considerations have motivated the study of an effective $(2+1)\,d$ relativistic field theory with N_f fermion flavors for the low-energy electronic excitations ($N_f = 2$ for monolayer graphene) and an instantaneous Coulomb interaction between conserved charges, to be reviewed in Sec. II below.[2–4] For sufficiently strong coupling the theory describes a quantum critical point (QCP) at $T = 0$ separating a semimetal phase in which charge carriers remain ungapped, from an insulating phase in which electron-hole exciton pairs condense in the ground state, inducing a gap at the Dirac points. It is conceivable that the properties of the QCP dominate the effective description of low-energy charge transport in graphene irrespective of whether the semimetal or insulating phase is physically realized.

Since the theory is strongly interacting, various nonperturbative approaches have been applied, including Monte Carlo simulation of an effective lattice field theory postulated to belong to the same universality class at the QCP. In a series of papers, Drut and Lähde[5] have simulated a graphene field theory with staggered lattice fermions in which electrostatic degrees of freedom are formulated on a $(3+1)$-dimensional lattice, while the electron fields are restricted to a $(2+1)$-dimensional slice. Their results favor the scenario that suspended graphene with $\alpha_{\mathrm{eff}} = 2.16$ is an insulator. More recent simulations with an improved fermion action support this scenario.[6] Two of us[7] have simulated an entirely $2+1$-dimensional model, which is in essence a noncovariant form of the Thirring model,[8] and showed that at infinite coupling for $N_f < N_{fc} = 4.8(2)$ graphene is an insulator, whereas for $N_f > N_{fc}$ it is a semimetal. The results from simulations of the same model at finite coupling provided evidence that graphene in vacuum is an insulator,[9] in agreement with Refs. 5 and 6. More recently, the authors of Ref. 10 presented preliminary results from Monte Carlo simulations of the tight-binding Hamiltonian on a hexagonal lattice.

At nonzero temperature, universality arguments imply that the critical properties of a $(d+1)$-dimensional theory coincide with those of a d-dimensional classical spin model with the same symmetries. The contribution of nonzero Matsubara modes can be absorbed into nonuniversal aspects of the transition. Consequently, fermions which satisfy antiperiodic boundary conditions and do not have zero modes are expected to decouple from the scalar sector. The validity of the dimensional reduction was confirmed with accuracy in Monte Carlo simulations of fermionic field theories such as the $(2+1)\,d$ Gross-Neveu model[11] and the $(3+1)\,d$ Nambu−Jona-Lasinio (NJL) model[12] and strong coupling QCD.[13]

There has been compelling experimental evidence[14] that at constant low temperature graphene undergoes a Berezinskii-Kosterlitz-Thouless (BKT) phase transition[15] when the intensity of an external magnetic field is varied. The authors of Ref. 14 showed that the steep increase in the electrical resistance at the Dirac point as a function of the magnetic field fitted accurately the essential scaling relation of the BKT scenario. The BKT transition occurs in two-dimensional systems with a U(1) symmetry and is driven by the unbinding of vortices, as reviewed in Sec. III. The transition separates two phases, neither of which have long-range order: a low-temperature spin-wave phase where vortices and antivortices form bound states and a high-temperature plasmalike phase of unbound vortices and antivortices. An analytical approach based on solutions of self-consistent Schwinger-Dyson equations[16] predicted that the critical temperature is given by $T_{\rm BKT} = \pi\Upsilon(T_{\rm BKT})/2 \approx \Delta_0/8$, where $\Upsilon(T_{\rm BKT})$ is the helicity modulus or stiffness of the order parameter at the transition temperature and Δ_0 is the fermion mass gap at $T = 0$. However, care is needed since, as shown in Ref. 17 in a model of graphene in which the full global symmetry is U(4) (expected for QED_3 with $N_f = 2$) instead of U(1), the creation of "half vortices" is energetically more favorable over the usual vortices. As a result, the critical temperature is driven to a lower value $\tilde{T}_{\rm BKT} = \pi\Upsilon(T_{\rm BKT})/8 = T_{\rm BKT}/4$.

In this paper we present results from simulations of our Thirring-like graphene model[9] at nonzero temperature. As we show in Sec. II, on the lattice the remnant of the U(4)/U(2) $\otimes$ U(2) manifold in which the order parameter of the continuum theory assumes values in U(1); we therefore do not anticipate the existence of half vortices in our lattice model away from the continuum limit.

The temperature in the simulation is given by $T = 1/N_t a_t$, where N_t is the lattice temporal extent and a_t the temporal lattice spacing. In a model with anisotropic interactions we anticipate that the temporal (a_t) and spatial (a_s) lattice spacings are not equal for arbitrary interaction coupling; that is, the anisotropy factor a_s/a_t is renormalized by quantum corrections governed by an action which treats time and space on a different footing. This has to be taken into account whenever deriving relations between physical quantities based on lattice observables; fortunately, for the current study all quantities can be expressed in units of the temporal lattice spacing a_t.

Furthermore, as we show in Sec. IV A the transition temperature in natural units is very low; that is, $T/\Delta_0 \ll 1$. This drives the critical coupling at which the BKT phase transition occurs to a very strong value (close to the strong coupling limit) even when the temporal lattice size $N_t = 32$. This value of N_t is much larger than the values $N_t = 6, \ldots, 10$ usually used in simulations of nonzero temperature QCD, and makes the study of the BKT scenario in graphene a computationally very difficult problem. On the basis of large-N_f arguments,[7] we believe that at very strong couplings our Thirring-like model should become similar to the instantaneous Coulomb interaction model.[4,5]

The main goals of this work are: (i) to measure $T_{\rm BKT}/\Delta_0$; (ii) to obtain a measurement of the helicity modulus $\Upsilon(T)$ for $T > T_{\rm BKT}$ and to compare with theoretical expectations; (iii) to measure the fermion mass gap Δ_T for $T > T_{\rm BKT}$ and to demonstrate that it remains nonzero even in the absence of long-range order through exciton condensation—this situation, which has been discussed theoretically in the context of the Gross-Neveu model,[18] is qualitatively similar to the pseudogap phase observed in the phase diagram of cuprate superconductors below optimal doping.

The paper is organized as follows: In Sec. II we present both the continuum model and the lattice formulation used here, along with a discussion of its global symmetries and breaking patterns. In Sec. III we briefly review the classic BKT theory of the thermal phase transition in planar models with U(1) global symmetry and discuss modifications if the global symmetry is expanded. In Sec. IV we present our simulation results, and in Sec. V we summarize and discuss our conclusions.

II. FORMULATION OF THE MODEL

Our starting point is a model of relativistic Dirac fermions moving in $2+1$ dimensions and interacting via an instantaneous Coulomb interaction. In Euclidean metric the action is[3,4,16]

$$S_1 = \sum_{a=1}^{N_f} \int dx_0 d^2x (\bar{\psi}_a \gamma_0 \partial_0 \psi_a + v_F \bar{\psi}_a \vec{\gamma}.\vec{\nabla}\psi_a + iV\bar{\psi}_a\gamma_0\psi_a) + \frac{1}{2e^2}\int dx_0 d^3x (\partial_i V)^2, \quad (1)$$

where e is the electron charge, v_F the Fermi velocity, V the electrostatic potential, and the 4×4 Dirac matrices satisfy $\{\gamma_\mu, \gamma_\nu\} = 2\delta_{\mu\nu}$, $\mu = 0, \ldots, 3$ [note γ_3 does not appear in (1)]. For monolayer graphene the number of fermion flavors is $N_f = 2$.

For sufficiently large coupling e^2 the description in terms of massless relativistic excitations may be disrupted by condensation of bound fermion-hole exciton pairs in the ground state, signaled by an order parameter $\langle\bar{\psi}\psi\rangle \neq 0$, with the result that a gap appears in the fermion spectrum, corresponding to a transition from a conductor to an insulator. The spontaneously broken global symmetry is U($2N_f$) generated by rotations of the form $\psi \mapsto UV\psi$, $\bar{\psi} \mapsto \bar{\psi}U^\dagger\gamma_3\gamma_5 V^\dagger\gamma_5\gamma_3$, with U acting on flavor indices $a = 1, \ldots, N_f$ and V a 2×2 matrix generated by the set $\{\mathbb{1}, \gamma_3, \gamma_5, i\gamma_3\gamma_5\}$, where $\{\gamma_\mu, \gamma_5\} = 0\ \forall\ \mu$. The order parameter remains invariant under independent U(N_f) rotations generated by both $\mathbb{1}$ and $i\gamma_3\gamma_5$, resulting in a breaking pattern,

$$\mathrm{U}(2N_f) \to \mathrm{U}(N_f) \otimes \mathrm{U}(N_f). \quad (2)$$

At zero temperature, for $N_f < N_{fc}$ the model predicts a finite sequence of QCPs whose properties at the critical coupling $e_c^2(N_f)$ depend on N_f (Ref. 4). The ground state is then an excitonic condensate for $e^2 > e_c^2$. Numerical simulations of the lattice model described below find $N_{fc} \simeq 5$ (Ref. 7). The QCP is an ultraviolet-stable fixed point of the renormalization group, implying a divergent correlation length and algebraic behavior of correlation functions which in principle may be distinct from that of free-field theory. If the physical value of e^2 in graphene were numerically close to the fixed-point value, in either subcritical or supercritical regimes, then the QCP might dominate the behavior of low-energy charged excitations, with

profound impact on the description of transport. Ultimately, this must be settled by experiment.

The possible relevance of a QCP has motivated the application of lattice gauge theory simulation techniques to the study of graphene. In this paper, we study a model discretized on a $2+1$-dimensional Euclidean cubic lattice with action which for $N_f = 2$ can be written in the staggered fermion formulation in the form (with bare Fermi velocity $v_F = 1$)[7,9]

$$\begin{aligned} S_{\text{latt}} = & \frac{1}{2}\sum_{x\mu i} \bar{\chi}^i_x \eta_{\mu x}(1 + i\delta_{\mu 0} V_x)\chi^i_{x+\hat{\mu}} \\ & - \bar{\chi}^i_x \eta_{\mu x}(1 - i\delta_{\mu 0} V_{x-\hat{0}})\chi^i_{x-\hat{\mu}} \\ & + m\sum_{xi} \bar{\chi}^i_x \chi^i_x + \frac{1}{4g^2}\sum_x V_x^2. \end{aligned} \tag{3}$$

Here χ, $\bar{\chi}$ are single-component Grassmann fermion fields defined on lattice sites, m an artificial mass gap introduced to regularize IR fluctuations on a finite system volume, and V a boson field, which mimics the electric potential of (1) in the limit $g^2 \to \infty$, defined on the links emanating from the sites in the timelike direction. The Kawamoto-Smit phases $\eta_{\mu x} = (-1)^{x_0+\cdots+x_{\mu-1}}$ are lattice analogs of the Dirac γ matrices. Note that V_x couples to a charge density J_{0x} which is the timelike component of a conserved current $J_{\mu x} = \frac{i\eta_{\mu x}}{2}[\bar{\chi}_x \chi_{x+\hat{\mu}} + \bar{\chi}_x \chi_{x-\hat{\mu}}]$. Since V appears in Gaussian form it may be integrated out to yield a model of self-interacting fermions resembling the Thirring model, with a local interaction term of the form $g^2 J_{0x}^2$. For finite g^2 the V field couples to a light, tightly bound electron-hole meson,[8] which becomes massless in the limit $g^2 \to \infty$ (Ref. 7), yielding identical dynamics to the electric potential of the gauge theory (1). The simulation results presented in Sec. IV were obtained not far from this limit.

A distinct model, with an identical $(2+1)\,d$ fermion sector this time interacting with Abelian lattice gauge fields defined on a $(3+1)$-dimensional lattice, has been studied by Drut and Lähde.[5] Their formulation is designed to reproduce the action (1), which describes a long-ranged Coulomb interaction between charges. Two comments about the relation between the models are worth making.

(i) The fermionic sectors share the same global symmetries. In the weakly coupled long-wavelength limit (3) describes $N_f = 2$ four-component Dirac fermions.[19]

(ii) The continuum theories modeled coincide in the strong coupling ($e^2, g^2 \to \infty$) and/or large-N_f limits.

In particular, the estimate $N_{fc} = 4.8(2)$ obtained using (3) is expected to hold for both models.[5,7]

Next we discuss symmetry breaking in the model (3). In the limit $m \to 0$ there is a global "chiral" symmetry

$$\chi_x \mapsto \exp(i\alpha\varepsilon_x)\chi_x; \quad \bar{\chi}_x \mapsto \exp(i\alpha\varepsilon_x)\bar{\chi}_x, \tag{4}$$

where $\varepsilon_x \equiv (-1)^{x_0+x_1+x_2}$, the lattice analog of γ_5, distinguishes odd and even sublattices. For N species of lattice fermion corresponding to $N_f = 2N$ continuum flavors, excitonic condensation of the form $\langle\bar{\chi}\chi\rangle \equiv V^{-1}\partial \ln \mathcal{Z}/\partial m \neq 0$ ($\mathcal{Z}$ is the partition function on the Euclidean space-time lattice) induces a spontaneous symmetry breaking of the form

$$\mathrm{U}(N_f/2) \otimes \mathrm{U}(N_f/2) \to \mathrm{U}(N_f/2). \tag{5}$$

Only in the weak-coupling continuum limit must we necessarily expect a restoration of the continuum breaking pattern (2), implying in particular that $\frac{7}{4}N_f^2$ would-be Goldstone modes remain massive for nonzero lattice spacing.[20] At the QCP, however, weak coupling cannot be assumed; moreover, the effective theory need not even be Lorentz invariant. It remains unclear, therefore, whether the enhanced symmetry of (1) will be fully restored, and a more systematic study of the discretized action as advocated in Ref. 6 will ultimately be needed to resolve this issue.

Finally, we mention an important technical issue concerning the model (3) which does not apply to the gauge-theory formulation.[5] For the action (3) there is no symmetry guaranteeing transversity of the vacuum polarization tensor (i.e., $\Delta^-_\mu \Pi_{\mu\nu x} \neq 0$, where Δ^-_μ is the backward difference operator), resulting in an additive renormalization of the coupling g^2:

$$g_R^2 = \frac{g^2}{1 - g^2/g^2_{\text{lim}}}, \tag{6}$$

where $g^2_{\text{lim}}(N_f) < \infty$ defines the effective location of the strong coupling limit. Unitarity is violated for $g^2 > g^2_{\text{lim}}$. In Refs. 7 and 21 g^2_{lim} was identified numerically with g^{-2}_{peak} defined by the (m- and volume-independent) location of a peak in the order parameter $\langle\bar{\chi}\chi\rangle$ found in the broken symmetry phase.

III. THEORETICAL EXPECTATIONS AT NONZERO TEMPERATURE

In the excitonic phase which forms at $T = 0$ for $g^2 > g_c^2$, for $N_f = 2$ the order parameter $\langle\bar{\chi}\chi\rangle \equiv \phi = \phi_0 e^{i\theta}$ spontaneously breaks a U(1) global symmetry of the action (3). For $T > 0$ long-range order is forbidden by the Coleman-Mermin-Wagner theorem;[22] rather, we expect at low T a phase where low-energy phase fluctuations are described by an effective Hamiltonian

$$H_{\text{eff}} \propto \frac{1}{2}(\vec{\nabla}\phi)^* \cdot (\vec{\nabla}\phi) \approx \frac{\Upsilon}{2}(\vec{\nabla}\theta)^2, \tag{7}$$

where in this context the parameter Υ is called the *helicity modulus*, and correlation functions decay algebraically:

$$\lim_{m\to 0}\langle\phi(0)\phi^\dagger(r)\rangle = \phi_0^2\langle e^{i\theta(0)}e^{-i\theta(r)}\rangle \propto r^{-\eta}, \tag{8}$$

with critical exponent $\eta = T/(2\pi\Upsilon)$. As temperature rises topologically nontrivial excitations become important. A vortex of charge q has the form (in polar coordinates r, ψ) $\theta = q\psi$, $|\vec{\nabla}\theta| = q/r$, and energy

$$E_q = \pi\Upsilon q^2 \ln\frac{L_s}{a_s}, \tag{9}$$

where L_s is the spatial extent of the universe and a_s the lattice spacing. Overall charge neutrality is thus a requirement at low T if E is to remain finite. Since a vortex can be located at any one of $(L_s/a_s)^2$ (dual) lattice sites, the entropy

$$S = 2\ln\frac{L_s}{a_s}. \tag{10}$$

The free energy $F = E - TS$ of a $|q| = 1$ vortex thus changes sign at a critical temperature

$$T_{\rm BKT} = \frac{\pi}{2}\Upsilon. \tag{11}$$

This is the celebrated BKT transition[15] between a low-T critical phase in which vortices can only exist in tightly bound dipole pairs, and a gapped phase where unbound vortices form a "topological plasma" which screens the long-range inter-vortex interaction.

The relation (11) remains true in a more sophisticated renormalization group treatment,[23] except that Υ must be replaced by its screened value $\Upsilon(T_{\rm BKT})$ exactly at the transition. The critical exponent η describing correlations for $T < T_{\rm BKT}$ thus obeys

$$\eta < \eta_c = \tfrac{1}{4}. \tag{12}$$

A related exponent δ describes the response of the order parameter to a small symmetry-breaking explicit mass gap m via $\langle\phi\rangle \propto m^{\frac{1}{\delta}}$. It is related to η via the hyperscaling relation $\delta = (4-\eta)/\eta$, yielding

$$\delta > \delta_c = 15. \tag{13}$$

This picture may need modification when applied to (1). Aleiner *et al.*[17] have performed a similar analysis for the U(2)-valued $\langle\bar\psi\psi\rangle$ using a Hamiltonian with independent moduli for U(1)- and SU(2)-valued fluctuations of the order parameter field. The crucial point is that the SU(2) σ model is asymptotically free, implying that $\Upsilon_{\rm SU(2)}$ rapidly runs to zero as high-momentum modes are integrated out, with the result that the U(1) effective Hamiltonian (7) is adequate for describing physics at large distances. However, the richer symmetry of the order parameter permits the existence of a new kind of topological excitation called a half-vortex with $q = \pm\frac{1}{2}$, whose energy is still given by (9), and which is thus much more readily formed by thermal fluctuations. The BKT transition temperature is accordingly modified to

$$\tilde T_{\rm BKT} = \frac{\pi}{8}\Upsilon, \tag{14}$$

with new values $\eta_c = \frac{1}{16}$ and $\delta_c = 63$.

IV. NUMERICAL RESULTS

In this section we present results from our numerical investigation of the model discussed in the previous section at nonzero temperature. More specifically we estimate the physical critical temperature, detect fermion mass generation in the high temperature phase and study the behavior of Υ at high T. In Euclidean field theory the temperature T is related to the time-extent L_t of the universe via $T = L_t^{-1} = (N_t a_t)^{-1}$ where in the second step a timelike lattice spacing a_t is specified. In general, numerical simulations are performed with N_t fixed, so that T is varied through variation of $a_t(g^2)$. Since $a_t \to 0$ at the QCP located at the bulk critical point g_c^2, we deduce that in the semimetal phase the range $0 < T < \infty$ maps to the range $0 < g^2 < g_c^2$, whereas in the insulating phase the same temperature range is mapped to $\infty > g^2 > g_c^2$. In this paper we are concerned with the latter case; bearing in mind the usual convention of presenting results in terms on inverse coupling, and also the additive coupling renormalization described in the previous section, we therefore are working in the range $g_{\rm lim}^{-2} < g^{-2} < g_c^{-2}$.

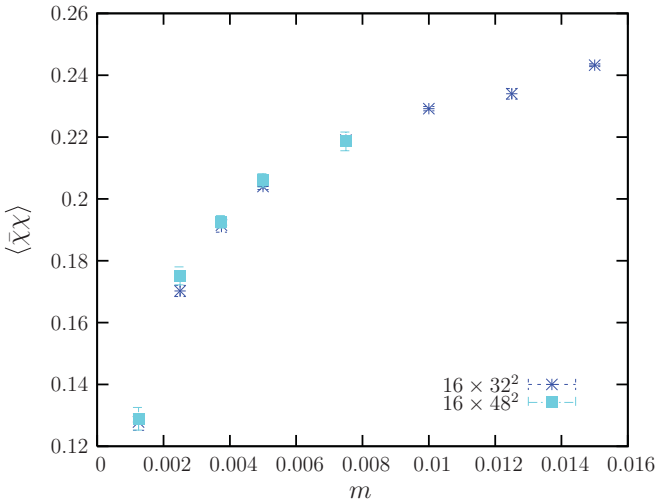

FIG. 1. (Color online) Exciton condensate $\langle\bar\chi\chi\rangle$ versus m from simulations at $g^{-2} = 0.375$ on 16×32^2 and 16×48^2 lattices.

A. BKT transition

The first set of simulations was performed with a lattice temporal extent $N_t = 16$ and spatial extents $N_s = 32,48$. For these lattice volumes $g_{\rm peak}^{-2} \approx 0.375$; recall that the value $g_{\rm lim}^{-2}$ corresponding to the infinite coupling limit has previously been identified with $g_{\rm peak}^{-2}$. However, this value of $g_{\rm peak}^{-2}$ is higher than the value $g_{\rm peak}^{-2} \approx 0.30(2)$ found at $T = 0$[7]. Although the existence of $g_{\rm peak}^{-2}$ defining the effective strong coupling limit is a ultraviolet (UV) artifact and therefore should not depend on N_t, when N_t is comparable to the lattice spacing a_t; that is, the UV scale becomes comparable to the IR scale, then it becomes difficult to disentangle the bulk and thermal transitions. In Fig. 1 we present results for the exciton condensate $\langle\bar\chi\chi\rangle$ versus m for $N_s = 32,48$ and $g^{-2} = 0.375$. It appears that finite volume effects are negligible down to $m = 0.001\,25$. We then fitted the data at $g^{-2} = 0.375,0.400$ from simulations on a 16×32^2 lattice to the scaling relation:

$$\langle\bar\chi\chi\rangle = Cm^{1/\delta}. \tag{15}$$

At the critical temperature $T_{\rm BKT}$ we expect $\delta = 15$. The results for the exponent δ and the fit qualities (χ^2/dof) are presented in Table I. The data and the fitted curves are shown in Fig. 2. The very low fit qualities and the values of $\delta = 5.5(1)$ and $5.1(1)$ for $g^{-2} = 0.375$ and 0.400, respectively, imply that even at $g_{\rm peak}^{-2}$ the temperature is higher than $T_{\rm BKT}$: We can never go down to $T_{\rm BKT}$ in simulations with $N_t = 16$.

TABLE I. Results from fits of $\langle\bar\chi\chi\rangle$ vs m from simulations on 16×32^2 lattices.

g^{-2}	δ	χ^2/dof
0.375	5.5(1)	30
0.400	5.1(1)	31

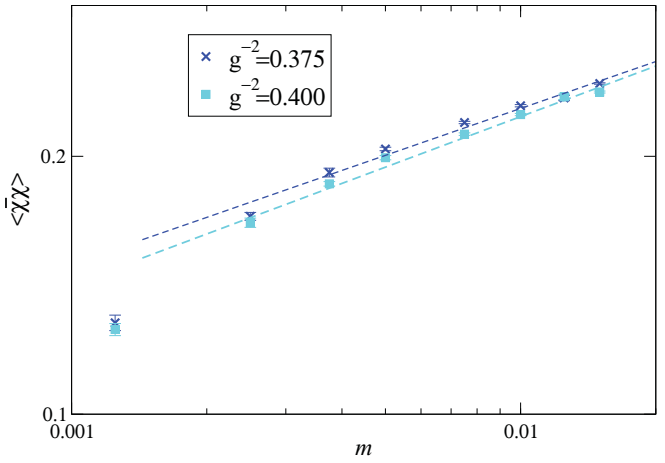

FIG. 2. (Color online) $\langle \bar{\chi}\chi \rangle$ versus m from a 16×32^2 lattice.

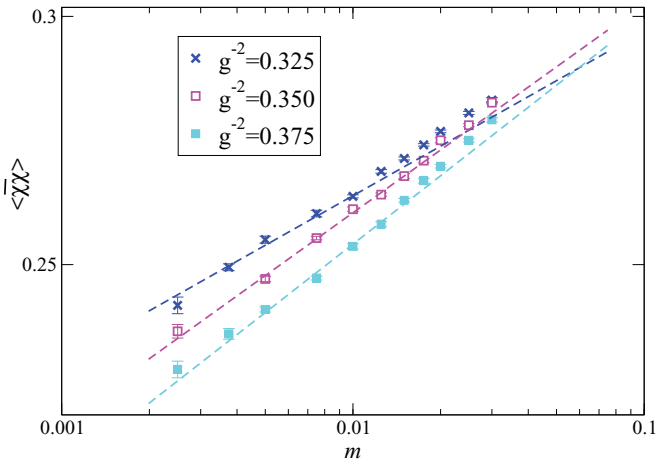

FIG. 3. (Color online) $\langle \bar{\chi}\chi \rangle$ versus m from a 32×64^2 lattice.

These preliminary simulations teach us that it will require very large lattices to identify a BKT transition. In order to approach $T_{\rm BKT}$ we tried $N_t = 32$ and $N_s = 64$. The simulations on such a large lattice at strong couplings required enormous computational time because the number of iterations of the conjugate gradient algorithm required for the inversion of the Dirac matrix kernel of (3) increased dramatically. For this reason it has not proved possible to identify a transition via singular behavior of the susceptibility $\partial\langle\bar{\chi}\chi\rangle/\partial m$ or the specific heat as was done, say, for fermion pairing leading to long-ranged phase coherence in the $(2+1)d$ Gross-Neveu model,[24] with $T_{\rm BKT}/\Delta_0 \approx 0.5$, using $N_t = 4$, $N_s = 30, \ldots, 150$.

Our strategy for locating $T_{\rm BKT}$ is therefore based entirely on the critical scaling relation (15). The data for $\langle\bar{\chi}\chi\rangle$ versus m were fitted to (15) for the ranges $m = 0.0025, \ldots, 0.010$ for $g^{-2} = 0.325$, $m = 0.0025, \ldots, 0.0175$ for $g^{-2} = 0.350$ and $m = 0.0025, \ldots, 0.015$ for $g^{-2} = 0.375$. The results are presented in Table II and Fig. 3 shows the data and the fitted curves. The value of $\delta = 15.0(3)$ found at $g^{-2} = 0.350$ implies that the BKT transition occurs at this coupling. It increases to 19.1(8) at $g^{-2} = 0.325$, which corresponds to a larger lattice spacing a_t and hence lower T, consistent with the BKT scenario. Note also that at the lowest temperature ($g^{-2} = 0.325$) the scaling region shrinks as compared to higher T ($g^{-2} = 0.350$), because as m increases the system crosses over to the $T = 0$ scaling. The slightly increased χ^2/dof for $g^{-2} = 0.375$ provides evidence that for $g^{-2} > 0.350$ the critical scaling based on (15) is not valid because this coupling lies in the high-temperature phase.

In order to eliminate the lattice spacing and estimate the physical critical temperature at the BKT transition we measured the $T = 0$ fermion mass at $g^{-2} = 0.350$. Using point sources we calculated the zero-momentum fermion time-slice correlator

$$C_f(t) = \sum_{\vec{x}\ \text{even}} \langle \chi_{\vec{0},0} \bar{\chi}_{\vec{x},t} \rangle, \tag{16}$$

where "even" refers to sites with spatial coordinate $\vec{x}$ obeying $(-1)^{x_1} = (-1)^{x_2} = 1$. This restriction improves the signal-to-noise ratio and originates in the observation that the action (3) is invariant only under translations by an even number of lattice spacings. The simulations were performed on cold lattices with $N_t = 48$ and $N_s = 24$ for $m = 0.01, 0.02, 0.03$. In Fig. 4 we present the data for $C_f(t)$ for $m = 0.01$. The fermion correlator data were fitted to

$$C_f(t) = A[\exp(-M_f t) - (-1)^t \exp(-M_f(N_t - t))]. \tag{17}$$

This form assumes that the spectral density $\rho(s)$ is saturated by a pole at $s = M_f^2$ in both particle and hole branches, appropriate for zero doping. In practice, this assumption is justified by the quality of the fit, evident in Fig. 4. The minus

TABLE II. Results from fits of $\langle\bar{\chi}\chi\rangle$ vs m from simulations on 32×64^2 lattices.

g^{-2}	δ	χ^2/dof
0.325	19.1(8)	1.7
0.350	15.0(3)	1.5
0.375	13.8(3)	3.9

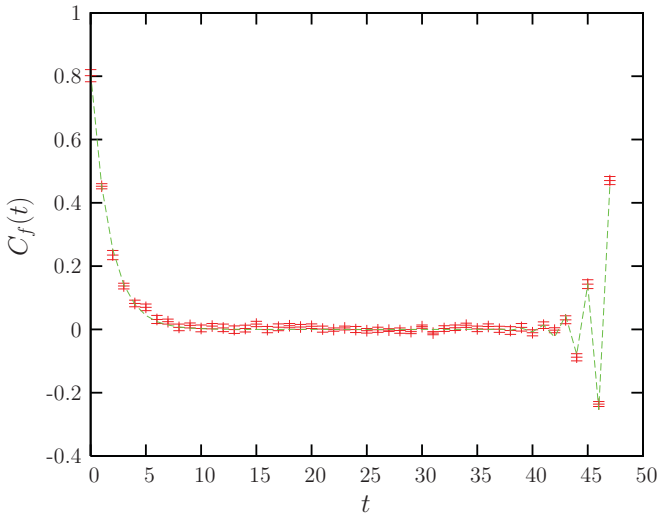

FIG. 4. (Color online) Fermion correlator for $g^{-2} = 0.35, m = 0.01$ on a 48×24^2 lattice.

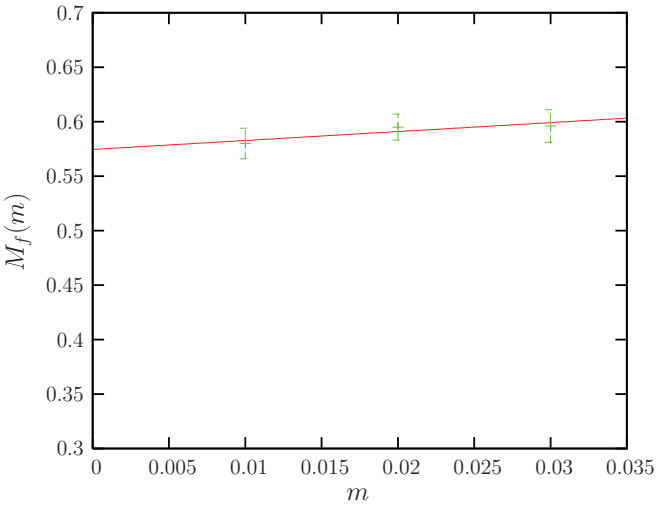

FIG. 5. (Color online) Fermion mass gap $M_f(m)$ versus m from simulations with $g^{-2} = 0.35, 0.375$ on a 48×24^2 lattice.

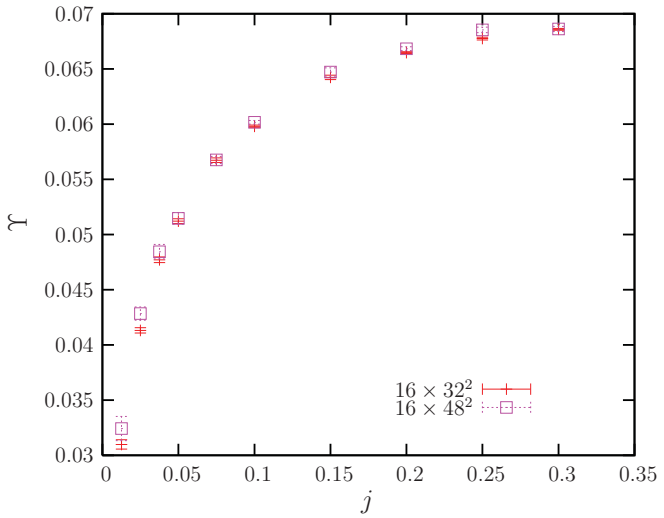

FIG. 6. (Color online) Υ versus j from simulations with $g^{-2} = 0.45$, $m = 0.001\,25$ on 16×32^2 and 16×48^2 lattices.

sign between the forward and backward terms is due to our choice of antiperiodic boundary conditions in the timelike direction. The values $M_f(m)$ extracted from fits to (17) were fitted to a linear scaling relation $M_f(m) = \Delta_0 + a_1 m$, where Δ_0 is the mass gap. The data and the fitted line is shown in Fig. 5. The extrapolation to $m = 0$ at $g^{-2} = 0.35$ yields $\Delta_0 a_t = 0.57(2)$. The physical estimate for the BKT temperature is then given by

$$\frac{T_{\rm BKT}}{\Delta_0} \equiv \frac{1}{N_t \Delta_0} = 0.055(2). \tag{18}$$

This result is slightly below half of the analytical prediction $T_{\rm BKT}/\Delta_0 \approx 1/8$ obtained by self-consistent solution of Schwinger-Dyson equations in Ref. 16. It is only possible to convert it into physical units indirectly, using the estimate $\Delta_0 \approx 35$ meV obtained in Ref. 25 by modeling the T dependence of electrical conductivity measured in suspended graphene samples.[26] This yields $T_{\rm BKT} \approx 20$ K. It should be stressed that this result has still to be extrapolated to the continuum limit $N_t \to \infty$, $a_t \to 0$. Another factor to bear in mind once lattice discretization artifacts disappear is that the U(4) global symmetry of the continuum model (1) will be recovered. In that case, as described in Sec. III the critical temperature $\tilde{T}_{\rm BKT}$ will be smaller than the value (18) by a factor of four, because half vortices will become energetically favored and dominate the disruption of long-range phase coherence.[17]

B. Helicity modulus

Next we present numerical estimates of $\Upsilon(T)$: We briefly review the method, adapted from Ref. 27. The mass term in (3) is replaced by a spatially varying source of the form $j \exp(i\theta(\vec{x})\varepsilon_x)$, where the single-valued phase is defined by

$$\theta(x_1, x_2) = \frac{2\pi}{N_s}(n_1 x_1 + n_2 x_2). \tag{19}$$

The helicity modulus parametrizes the response of the axial current $J^a_{\mu x} = \frac{i\eta_{\mu x}}{2}[\bar{\chi}_x(\varepsilon\chi)_{x+\hat{\mu}} + \bar{\chi}_x(\varepsilon\chi)_{x-\hat{\mu}}]$, which is conserved in the limit $j \to 0$:

$$\vec{J}^a(j) = \Upsilon(j)\vec{\nabla}\theta = \frac{2\pi\Upsilon}{L_s}(n_1, n_2). \tag{20}$$

To make contact with the theoretical considerations discussed above requires the extrapolation $j \to 0$. Note that because $\vec{\nabla} \cdot \vec{J}^a$ has the same form as the kinetic energy term in the action (3), the dimensionless variables appearing in (20) are $\vec{J}^a a_s a_t$ and Υa_t, meaning that Υ naturally scales like a mass gap. In practice, to minimize discretization artifacts we choose $n_1 = 1$, $n_2 = 0$. For technical reasons associated with the choice $N_f = 2$, the results for Υ presented in this paper were calculated in the "partially quenched" approximation, in which equilibrated field configurations were generated using a spatially constant mass m, the spatially varying source only being introduced for the measurement of $\vec{J}^a$.

Given that Υ is noisier than $\langle\bar{\chi}\chi\rangle$ we restricted our simulations to a lattice with $N_t = 16$ and were therefore only able to study high temperatures. In Fig. 6 we present $\Upsilon(j)$ for $m = 0.001\,25$ and $g^{-2} = 0.45$ extracted from simulations with $L_s = 32$ and $L_s = 48$. It is inferred that effects due to finite L_s are small, in contrast to results from the Gross-Neveu model at nonzero baryon density with $T < T_{\rm BKT}$ (Ref. 27). In order to extract the $m = 0$ value of Υ for each value of j we performed linear extrapolations using $\Upsilon(m, j) = \Upsilon(m = 0, j) + a_2 m$. The results for $\Upsilon(m = 0, j)$ versus j for different $g^{-2} < g_c^{-2}$ corresponding to $T > T_{\rm BKT}$ are shown in Fig. 7.

Unfortunately, we do not have a model permitting a reliable extrapolation of these data to $j \to 0$. The data show a marked downward curvature as $j \to 0$ and it is therefore plausible, bearing in mind the insensitivity to L_s, that Υ vanishes in this limit, as expected for $T > T_{\rm BKT}$ (however, the figure, including the point where curves corresponding to differing temperatures intersect at $j \approx 0.125$, is qualitatively very similar to data taken with finite L_s and fixed $T < T_{\rm BKT}$ but varying baryon density in the $2+1d$ Gross-Neveu model[27]). For $j < 0.1$ there is a clear T dependence. For reference, Eq. (11) predicts

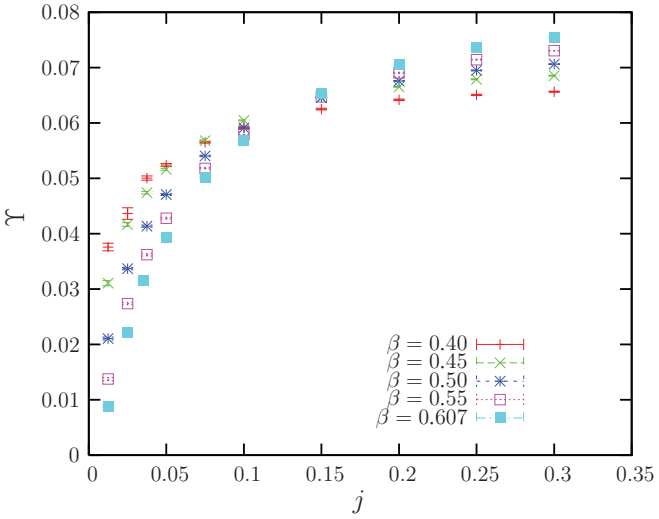

FIG. 7. (Color online) Chirally extrapolated Υ versus j for different values of g^{-2} extracted from simulations on a 16×32^2 lattice.

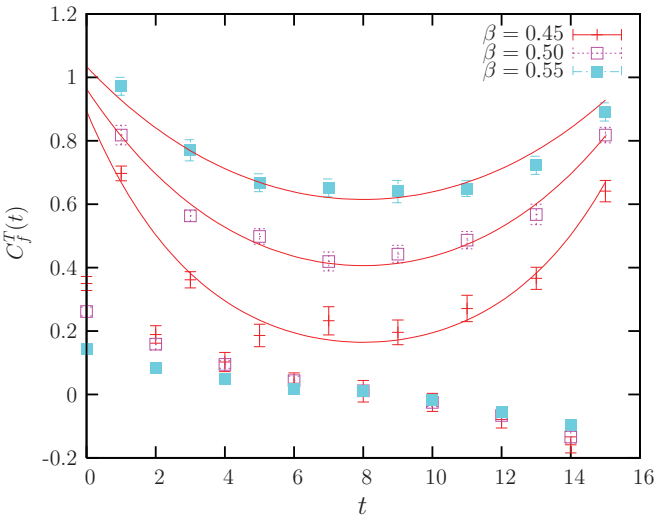

FIG. 8. (Color online) Fermion correlator with $m = 0.001\,25$ and $g^{-2} = 0.45, 0.50, 0.55$ on a 16×32^2 lattice. The curves result from fits to data with t odd.

$\Upsilon(T_{\rm BKT})a_t = 0.040$, of the same order of magnitude as $\Upsilon(j)$ around the "knee" seen in the data of Fig. 12 at $j \sim 0.1$; even though a quantitative description is still lacking, therefore, the signal for Υ is broadly consistent with the BKT scenario outlined in Sec. III.

C. Quasiparticle thermal mass and dispersion relation

Next we calculated the fermion thermal mass in the high-temperature region from simulations on 16×32^2 lattices. Once again, the fact that the fermion correlator has a smaller signal-to-noise ratio than the order parameter $\langle \bar{\chi}\chi \rangle$ forces us to work on smaller volumes. Now, at $T > 0$ fermions can acquire a nonzero thermal mass even in the absence of spontaneous symmetry breaking. For a weakly coupled theory, this is simply the Debye screening mass $m_D \sim gT$, but in a strongly coupled theory where dynamical mass generation at $T = 0$ results from spontaneous symmetry breaking, it is better to draw analogies with the "pseudogap" phase thought to form in cuprate superconductors at strong coupling or low carrier density.[18] Once again, we write the pairing field as $\bar{\chi}\chi = \phi_0 e^{i\theta}$. For a temperature range $T_{\rm BKT} < T < T^*$, the pseudogap phase arises due to the "local" gap modulus ϕ_0, neutral under U(1) rotations, remaining nonzero, while the phase θ fluctuates violently, precluding both a nonzero order parameter and also the long-ranged phase coherence signaled by a nonvanishing helicity modulus. In Ref. 18 the temperature T^* in the $(2+1)\,d$ Gross-Neveu model is predicted to coincide with the estimate $\Delta_0/2\ln 2$ given by mean-field theory, and the difference $T^* - T_{\rm BKT} \simeq (N_f \ln 2)^{-1}$. The existence of the pseudogap phase at nonzero temperature was demonstrated in numerical simulations of Gross-Neveu models with U(1) (Ref. 24) and SU(2) × SU(2) (Ref. 28) chiral symmetries and analytically in the $4d$ NJL model.[29]

In Fig. 8 we show the fermion time-slice correlator $C_f^T(t)$ for $g^{-2} = 0.45, 0.50, 55$ and $m = 0.001\,25$. We fitted the data for odd time slices only to

$$C_f^T(t) = A\big[\exp\big(-M_f^T t\big) + \exp\big(-(N_t - t)M_f^T t\big)\big]. \quad (21)$$

The small values of $C_f^T(t)$ observed on even time slices signals a manifest chiral symmetry which is broken only explicitly by the fermion bare mass term. The $\mathrm{U}(1)_\epsilon$ symmetry (4) of staggered fermions implies that the only nonvanishing elements of the propagator are C_{feo} and C_{foe}, where the e/o subscripts denote sites with $\varepsilon_x = \pm 1$.

In Fig. 9 we present the results for M_f^T versus m extrapolated with a linear function $M_f^T(m) = \Delta_T + a_3 m$ to the chiral limit. Figure 10 shows Δ_T versus g^{-2}. As g^{-2} increases the lattice spacing decreases and at the bulk critical coupling $g_c^{-2} = 0.609(2)$ $a_t = a_s = 0$[9], implying $T \to \infty$. It is clear from Fig. 10 that Δ_T remains of the same order of magnitude as Δ_0 for a significant extent of the high-temperature phase $T > T_{\rm BKT}$, lending strong support to the pseudogap scenario with $T^* > T_{\rm BKT}$.

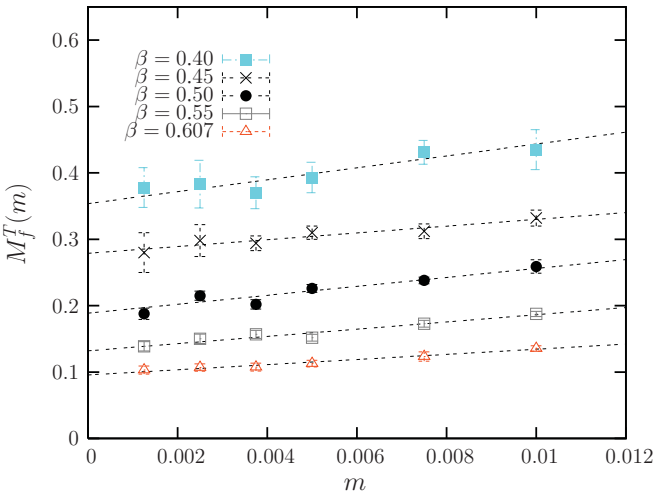

FIG. 9. (Color online) Fermion thermal mass M_f^T versus m for various g^{-2} extracted from simulations on a 16×32^2 lattice.

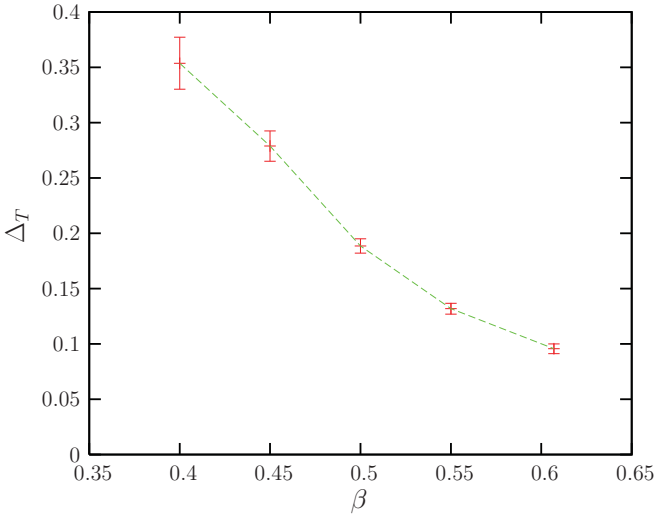

FIG. 10. (Color online) Chirally extrapolated thermal mass Δ_T versus g^{-2} extracted from simulations on a 16×32^2 lattice.

The fermion energy as a function of momentum is accessed via analysis of the Euclidean time-slice propagator $C_f(\vec{p},t)$ defined by

$$C_f^T(\vec{p},t) = \sum_{\vec{x}\ \text{even}} \langle \chi(\vec{0},0)\bar{\chi}(\vec{x},t)\rangle e^{-i\vec{p}.\vec{x}}, \tag{22}$$

where the components of momentum $\vec{p}$ take values $2\pi n/L_s$, with $n = 0,1,\ldots,L_s/4$. The energy $E(\vec{p})$ is then extracted by a fit of the form

$$C_f(\vec{p},t) = B(e^{-Et} + e^{-E(L_t-t)}), \tag{23}$$

where again only data with t odd were used. We measured $E(\vec{p})$ for $\vec{p} = (p_1,0)$ on 16×32^2 in the high-temperature phase. To proceed we parametrize the dispersion relation using

$$E(p) = A \sinh^{-1}(\sqrt{\sin^2 p + M^2}), \tag{24}$$

where for $A = 1$ and $M = m$ the exact result for noninteracting lattice fermions is recovered. Sample fits to (24) at $m = 0.005$ are shown in Fig. 11. The dispersion flattens out to have zero slope at the effective Brillouin zone edge at $p = \frac{\pi}{2}$; this flattening is a discretization artifact with no physical significance. For small M we can interpret $E(0) \equiv M_f^T \approx AM$ as the quasiparticle mass (or gap), and for small p in the limit $M \to 0$ then $dE/dp \approx A$ is the renormalized Fermi velocity $v_{FR}^T a_t/a_s$ at nonzero temperature, where we have restored explicit factors of lattice spacing. Without further information we are unable to distinguish between renormalization of the physical Fermi velocity and that of the cutoff anisotropy due to quantum corrections (this point was not realized in Ref. 9), but note that the latter must be T independent. Results for A as a function of m are shown in Fig. 12. Despite some noise in the data the parameter A, and hence v_{FR}^T, is both m- and g^{-2}-independent, taking a numerical value $\approx$0.65, which is very close to the value $A \approx 0.7$ reported in Ref. 9 at $T = 0$. This implies that the principal physical effect of the hot medium is to generate a nonzero thermal mass rather than to renormalize the Fermi velocity. A similar effect was observed in nonzero T simulations of the $(2+1)\,d$ Gross-Neveu model with an SU(2) $\otimes$ SU(2) chiral symmetry.[28]

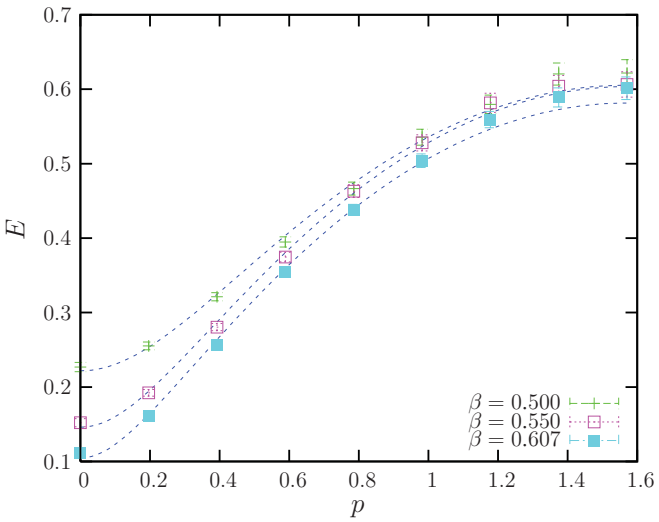

FIG. 11. (Color online) Quasiparticle dispersion relation $E(p)$ as measured on a 16×32^2 lattice with $m = 0.005$.

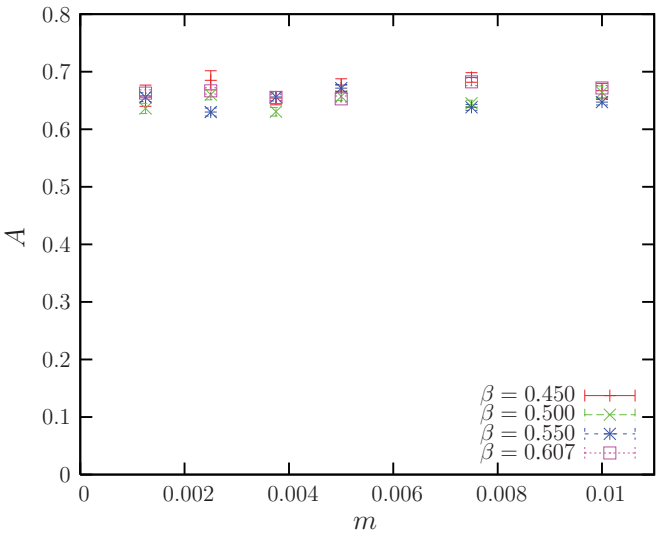

FIG. 12. (Color online) The fitted parameter A vs m for various values of g^{-2}.

V. SUMMARY AND CONCLUSION

The main result of this exploratory study of thermal effects in the insulating phase of the graphene effective theory (1) with $N_f = 2$, via numerical simulation of its discrete avatar (3), is the determination of the critical temperature for vortex unbinding $T_{\text{BKT}}/\Delta_0 \approx 0.06$. This value is considerably smaller than the ratio found in the Gross-Neveu model ($T_{\text{BKT}}/\Delta_0 \approx 0.5$),[24] underlining the point that different four-point Fermi interactions yield distinct dynamics in $(2+1)\,d$ and that perturbative approaches such as the $1/N_f$ expansion are unlikely to be accurate for graphene.[8] It also implies that study of the BKT transition in this system is a numerically challenging problem, requiring large lattice volumes in order to resolve the large separation of scales. With the resources at our disposal we have been able to work with $N_t = 32$,

which has enabled an estimate of $T_{\rm BKT}$ via the critical scaling (13) of the order parameter with external mass source and identification of the exponent δ, but not yet, it must be stressed, via direct observation of singular behavior in any thermodynamic observable. That said, it is noteworthy that our value (18) is not too far removed from predictions made using Schwinger-Dyson equations.[16]

Two major caveats must be noted. First, predictions made using the discrete model (3) can strictly only be applicable in the continuum limit; we therefore need to explore the limit $g^2 \searrow g_c^2$ to control the inevitable discretization artifacts, which may scale with nontrivial powers of a_s, a_t as the QCP is approached. Unfortunately, in practical terms this requires the limit $N_t \to \infty$. Second, as noted earlier, it is argued that in the continuum limit the global symmetry of the effective graphene Lagrangian enlarges from U(1)⊗U(1) to U(4), implying the existence of half-vortex topological excitations, which exhibit an unbinding transition at a still lower temperature $\tilde{T}_{\rm BKT} = T_{\rm BKT}/4$ (Ref. 17). Since our estimate of the critical temperature assumes the orthodox BKT scenario, we are unable to comment further on this possibility. Resolving this question will probably require a more refined lattice fermion discretization, as advocated in Ref. 6.

We have also presented results for the helicity modulus Υ as a function of the source strength j introduced to induce a circulating supercurrent in our system. The numerical challenge has so far restricted our study to the region $T > T_{\rm BKT}$, but the magnitude of $\Upsilon(j)$ observed is consistent with the expectations of the conventional BKT scenario. We are unaware of any effective model enabling a controlled $j \to 0$ extrapolation on finite systems.

Finally, the calculation of the quasiparticle propagator presented in Sec. IV C reveals the persistence of a gap $\Delta_T \lesssim \Delta_0$ for temperatures $T > T_{\rm BKT}$, despite the fact that the form of the correlators shown in Fig. 8 is characteristic of propagation through a chirally symmetric medium. As argued in Ref. 24, in this phase the fermion flips chirality, permitting propagation at speeds $v < v_F$, by constantly exchanging massless bosonic quanta with the medium: This is signaled by the spectral density function $\rho(s)$ being modified from a simple pole on the mass shell to a branch cut above the threshold at $s = \Delta_T^2$. The situation qualitatively resembles the discussion of the pseudogap phase in cuprates given in Ref. 18. In addition, the analysis of the fermion dispersion relation for $T > T_{\rm BKT}$ showed that the main effect of the hot medium is to generate a nonzero thermal quasiparticle mass rather than to renormalize the $T = 0$ physical Fermi velocity.

ACKNOWLEDGMENT

The authors wish to thank the Diamond Light Source for kindly allowing them to use extensive computing resources.

[1] A. H. Castro Neto, F. Guinea, N. M. R. Peres, K. S. Novoselov, and A. K. Geim, Rev. Mod. Phys. **81**, 109 (2009); N. M. R. Peres, *ibid.* **82**, 2673 (2010); D. S. L. Abergel, V. Apalkov, J. Berashevich, K. Ziegler, and T. Chakraborty, Adv. Phys. **59**, 261 (2010); S. Das Sarma, S. Adam, E. H. Hwang, and E. Rossi, Rev. Mod. Phys. **83**, 407 (2011); V. N. Kotov, B. Uchoa, V. M. Pereira, A. H. Castro Neto, and F. Guinea, e-print arXiv:1012.3484 (submitted to Rev. Mod. Phys.).

[2] D. V. Khveshchenko, Phys. Rev. Lett. **87**, 246802 (2001).

[3] E. V. Gorbar, V. P. Gusynin, V. A. Miransky, and I. A. Shovkovy, Phys. Rev. B **66**, 045108 (2002).

[4] D. T. Son, Phys. Rev. B **75**, 235423 (2007).

[5] J. E. Drut and T. A. Lähde, Phys. Rev. Lett. **102**, 026802 (2009); Phys. Rev. B **79**, 165425 (2009); **79**, 241405(R) (2009).

[6] J. Giedt, A. Skinner, and S. Nayak, Phys. Rev. B **83**, 045420 (2011); J. E. Drut, T. A. Lähde, and L. Suoranta, e-print arXiv:1002.1273 (to be published).

[7] S. Hands and C. Strouthos, Phys. Rev. B **78**, 165423 (2008).

[8] L. Del Debbio, S. J. Hands, and J. C. Mehegan, Nucl. Phys. B **502**, 269 (1997).

[9] W. Armour, S. Hands, and C. Strouthos, Phys. Rev. B **81**, 125105 (2010).

[10] R. C. Brower, C. Rebbi, and D. Schaich, e-print arXiv:1101.5131 (to be published).

[11] J. B. Kogut, M. A. Stephanov, and C. G. Strouthos, Phys. Rev. D **58**, 096001 (1998).

[12] S. Chandrasekharan, J. Cox, K. Holland, and U. J. Wiese, Nucl. Phys. B **576**, 481 (2000); S. Chandrasekharan and J. C. Osborn, Phys. Lett. B **496**, 122 (2000); C. G. Strouthos and S. Christofi, J. High Energy Phys. **01**, 057 (2005).

[13] S. Chandrasekharan and F. J. Jiang, Phys. Rev. D **68**, 091501 (2003); S. Chandrasekharan and C. G. Strouthos, *ibid.* **68**, 091502 (2003).

[14] J. G. Checkelsky, L. Li, and N. P. Ong, Phys. Rev. Lett. **100**, 206801 (2008); Phys. Rev. B **79**, 115434 (2009).

[15] V. L. Berezinskii, Sov. Phys. JETP **32**, 493 (1971); J. M. Kosterlitz and D. J. Thouless, J. Phys. C **5**, 124 (1972); J. Phys. C **6**, 1181 (1973).

[16] D. V. Khveshchenko, J. Phys. Condens. Matter **21**, 075303 (2009).

[17] I. L. Aleiner, D. E. Kharzeev, and A. M. Tsvelik, Phys. Rev. B **76**, 195415 (2007).

[18] E. Babaev, Phys. Lett. B **497**, 323 (2001).

[19] C. J. Burden and A. N. Burkitt, Europhys. Lett. **3**, 545 (1987).

[20] S. J. Hands, J. B. Kogut, L. Scorzato, and C. G. Strouthos, Phys. Rev. B **70**, 104501 (2004).

[21] S. Christofi, S. J. Hands, and C. G. Strouthos, Phys. Rev. D **75**, 101701(R) (2007).

[22] S. R. Coleman, Commun. Math. Phys. **31**, 259 (1973); N. D. Mermin and H. Wagner, Phys. Rev. Lett. **17**, 1133 (1966).

[23] D. R. Nelson and J. M. Kosterlitz, Phys. Rev. Lett. **39**, 1201 (1977); D. R. Nelson, in *Phase Transitions and Critical Phenomena*, edited by C. Domb and J. L. Lebowitz (Academic Press, London, 1983), Vol. 7, p. 1.

[24] S. J. Hands, J. B. Kogut, and C. G. Strouthos, Phys. Lett. B **515**, 407 (2001).

[25] J. E. Drut, T. A. Lähde, and E. Tölö, e-print arXiv:1005.5089 (to be published).

[26] K. I. Bolotin, K. J. Sikes, J. Hone, H. L. Stormer, and P. Kim, Phys. Rev. Lett. **101**, 096802 (2008).

[27] S. Hands and A. S. Sehra, Phys. Lett. B **637**, 229 (2006).

[28] C. G. Strouthos and D. N. Walters, Phys. Rev. D **67**, 034505 (2003).

[29] P. Castorina, G. Nardulli, and D. Zappala, Phys. Rev. D **72**, 076006 (2005).